Grünig, L.; Meyer, A.; Emmler, T.; Abetz, V.; Handge, U.:
Solvent-Induced Crystallization of Poly(phenylene sulfone).
In: Macromolecules. Vol. 54 (2021) 10, 4816 - 4826.

First published online by ACS: 07.05.2021

https://dx.doi.org/10.1021/acs.macromol.1c00323

Solvent-Induced Crystallization of Poly(phenylene sulfone)

Lara E. Grünig[1], Andreas Meyer[2], Thomas Emmler[1], Volker Abetz[1,2], Ulrich A. Handge[1,]*

[1] Helmholtz-Zentrum Geesthacht, Institute of Membrane Research, Max-Planck-Strasse 1, 21502 Geesthacht, Germany

[2] Universität Hamburg, Institute of Physical Chemistry, Grindelallee 117, 20146 Hamburg, Germany

Crystallization, poly(phenylene sulfone), solvent quality, wide angle X-ray scattering, NMR spectroscopy

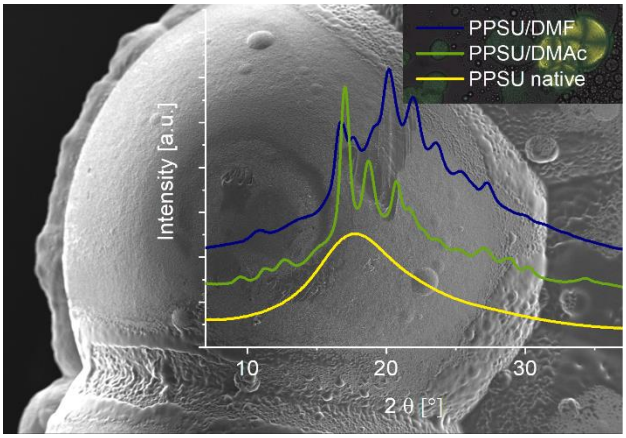

Figure: For Table of Contents Only

ABSTRACT. Crystallization of poly(phenylene sulfone) (PPSU) in various solvents was investigated. Poly(phenylene sulfone) is commonly classified as an amorphous polymer. However, crystallization of PPSU occurs given that the solvent quality is low. That may be the case through adding a non-solvent, like water or alcohol, to a good solvent like *N*-methyl-2-pyrrolidone (NMP), as it is often the case in recipes for membrane dope solutions, or by choosing a poor solvent like *N,N´*-dimethylacetamide (DMAc) or *N,N´*-dimethylformamide (DMF). The solvent quality moderates the nucleation as well as the growth mechanisms, resulting in different crystalline structures. Wide-angle X-ray scattering (WAXS) investigations revealed the degree of crystallinity for PPSU in solutions of DMAc and DMF, respectively. Poly(phenylene sulfone) in DMAc formed well defined banded spherulites that showed a typical maltesian cross in oberservations with polarized light microscopy. PPSU in DMF, however, crystallized with complete confinement of the solvent into the crystalline structure, so that no defined spherical objects grew. However, atomic force microscopy (AFM) investigations revealed crystalline plates. A thickness of 21 nm of a single plate was determined by the height profiles of AFM micrographs. The lattice spacing for both structures was calculated to be 5.3 Å. The surface of both, the plates and the spherulites, consists of lamellar fibrils with a thickness of 10 nm and a length in the order of 100-150 nm, as determined by scanning electron microscopy and AFM investigations. The authors propose the reason for the crystallization to be π-π-stacking of the rather stiff biphenylene groups. Nuclear magnetic resonance spectroscopy supported this assumption. The spectra showed peak broadening of the multiplets over time and a chemical shift to higher frequencies, implying distinct delocalization of electrons, as it is the case for interacting conjugated systems.

INTRODUCTION. Due to its high temperature stability and chemical resistance poly(phenylene sulfone) (PPSU) is of growing interest for various industrial applications. Just recently, PPSU has often been used not only for high temperature applications like foaming or 3D-printing [1-3], but also for the fabrication of nursing tools like baby bottles[4]. The combination of food-safety as well as the inherent chemical resistance makes PPSU a very promising candidate for membrane wastewater treatment[5-6], where regular chemical cleaning pits the polymer membranes and food-safety is of great importance. Promising approaches are the processing of PPSU to mixed-matrix membranes for ultra- or nanofiltration, equipped with nanoparticles or blending with miscible polymers for heavy metal removal, ion exchange or low fouling tendencies[7-14]. Of growing interest is not only the purification of liquids, but also of hydrogen, which was investigated by Naderi and coworkers for dual-layer hollow fiber membranes made of sulfonated PPSU[15-16]. Investigations leading to this study were intended to develop solutions for the fabrication of membranes based on PPSU. However, the viscoelastic properties of the corresponding solutions changed for PPSU solved in NMP and a non-solvent. The solutions turned turbid and apparent gelation occurred, which prevents the further use of the solution for membrane fabrication. To reproduce the change in the physical properties of the membrane dope solution, the system was reduced from a ternary to a binary system, by worsening the solvent quality and replacing *N*-methyl-2-pyrrolidone (NMP) and the non-solvent with *N,N´*-dimethylacetamide (DMAc) or *N,N´*-dimethylformamide (DMF). Usually PPSU is referred to be an amorphous polymer, so to the best of our knowledge no literature reporting on crystallinity of PPSU exists so far. Note, that sometimes authors abbreviate poly(1,4-phenylene sulfone), poly(*p*-phenylene sulfone) and poly(*p*-phenylene sufide) as PPSU[17-20]. However, these substances describe a different polymer, which does not contain any biphenylene units. Other groups reported in molecular dynamics simulations calculated attractive forces and

favored low spacing (0.5 nm) for two PPSU molecules, i.e., due to π–π-stacking of the biphenylene groups[21-22]. Similar assumptions were stated by Blackadder *et al.* for the origin of rarely observed crystalline parts in poly(ether sulfone)[23-24] or by Benhalima *et al.* who made suggestions for crystalline structures for modified poly(aryl ethers) and its oligomers[25-26]. Interestingly, a recent study observed reversible crystallization of poly(ether sulfone) in DMF combined with benzene as a non-solvent or when cooling the solution[27]. The solvent was captured into the crystalline structure, but by removing the solvent, the crystalline structures became disordered and turned amorphous. Phase separation of PPSU in poor solvents was observed before, but it has been interpreted as gelation[28]. Here, the authors report a detailed investigation of the solvent-induced crystallization of native PPSU in solutions with DMAc and DMF, respectively, as examples for PPSU crystallization in poor solvents. The degree of crystallinity was determined by wide-angle X-ray scattering (WAXS) measurements. The melting of the crystalline regions was investigated via polarized light microscopy (PLM) and differential scanning calorimetry (DSC) as well as the morphology via scanning electron (SEM) and atomic force microscopy (AFM). Nuclear magnetic resonance spectroscopy was performed to investigate the molecular interaction during the crystallization process. The new findings will support the ability to adjust the properties of materials fabricated with PPSU solutions in future applications.

EXPERIMENTAL SECTION.

Materials. Poly(phenylene sulfone) (Ultrason® P 3010) was kindly provided by BASF SE (Ludwigshafen, Germany) with an apparent weight average of the molecular weight (M_w) of 54 000 g mol^{-1}, as determined by gel permeation chromatography (GPC) in DMAc (calibrated to polystyrene). NMP, DMAc and DMF were purchased from Merck (Darmstadt, Germany) and used without further purification. The chemical structures of PPSU and the solvents are shown in

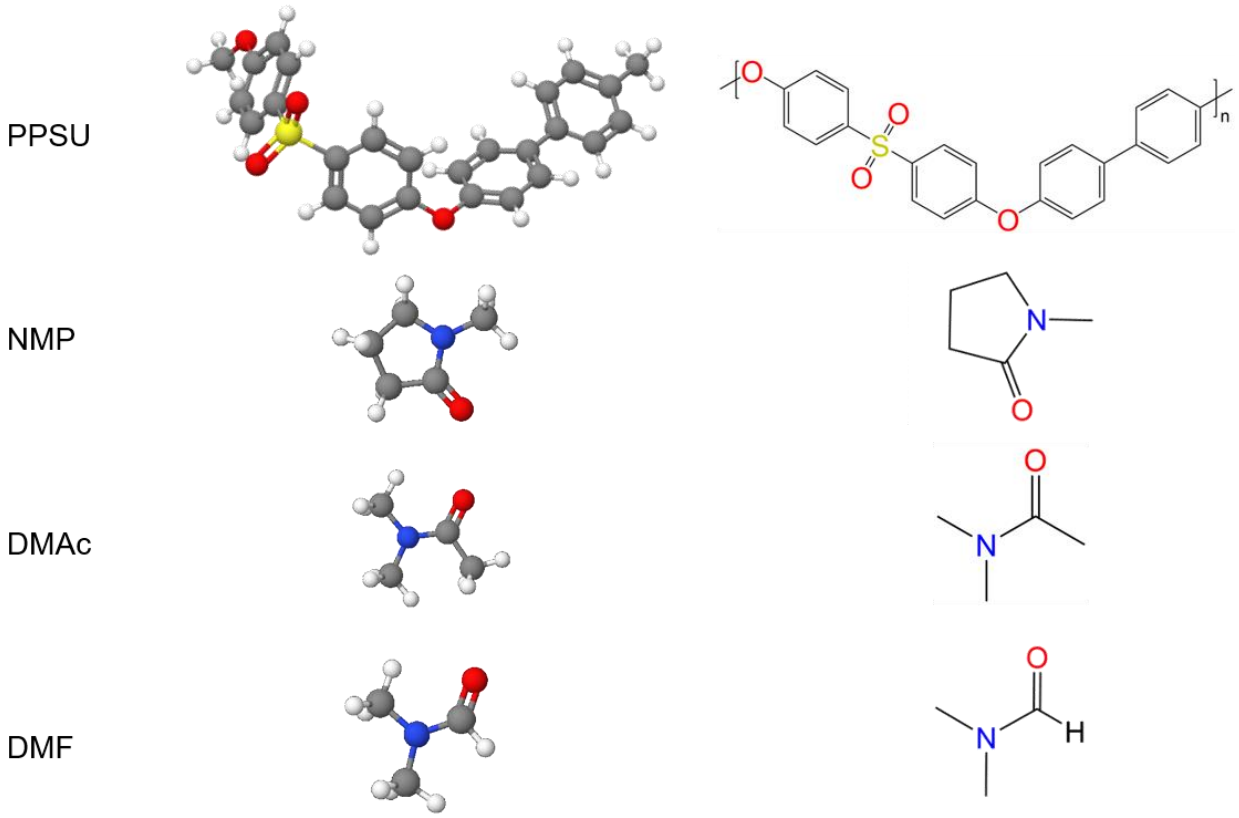

Figure 1.

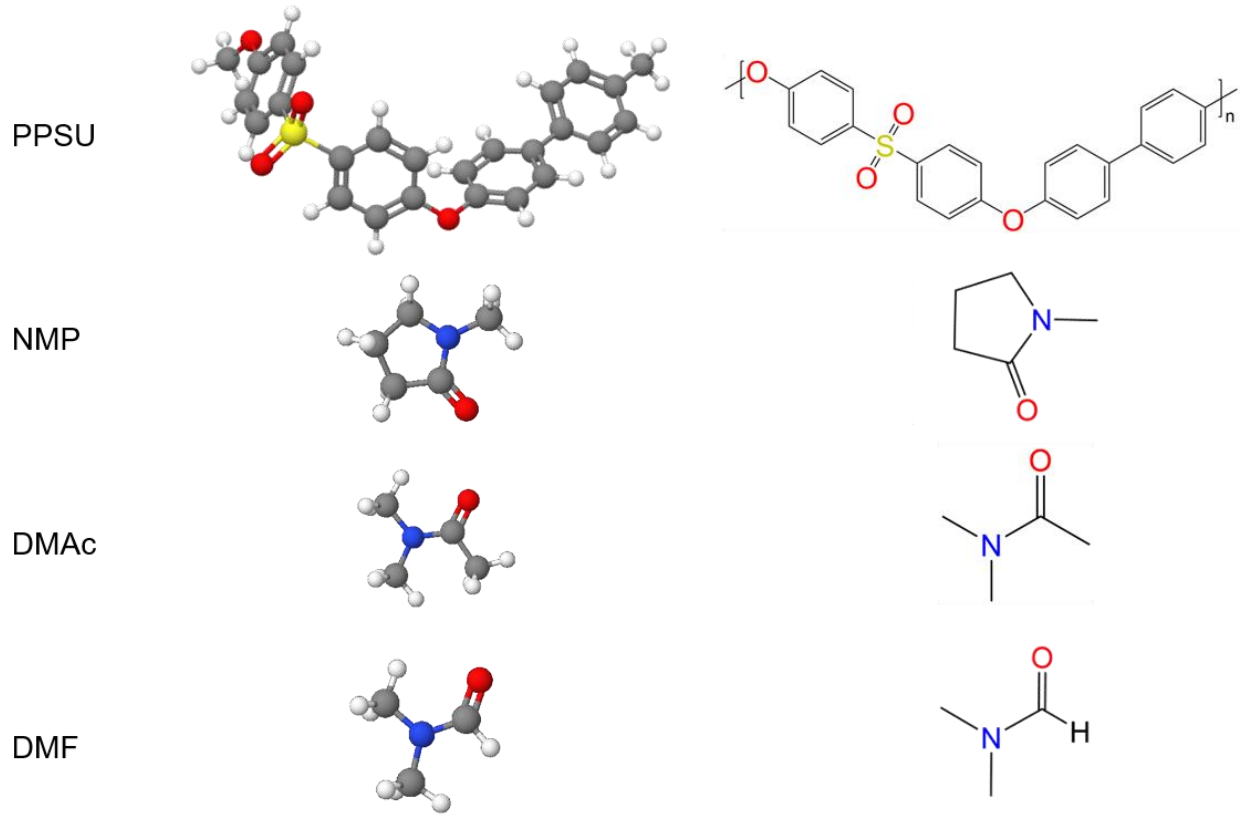

Figure 1. Chemical structure of poly(phenylene sulfone) (PPSU) and the solvents *N*-methyl-2-pyrrolidone (NMP), *N,N'*-dimethylacetamide (DMAc) and *N,N'*-dimethylformamide (DMF).

Solvent-Induced Crystallization. Solutions of PPSU in NMP, DMAc and DMF, respectively, were prepared and homogenized in a SpeedMixer™ DAC 800.2 (Hauschild & Co. KG, Hamm, Germany) at speeds of 200, 800 and 1200 rpm within 30 min of mixing time. The concentration of the investigated solutions was 25 wt. % and is given in weight percentage, if not specified else. The solutions were stored at 25 °C and protected from light. For AFM, SEM, PLM and selected WAXS and DSC measurements the crystallized polymer was dried under vacuum for 7 days at 70 °C. All other investigations on the crystallized solutions were performed without pretreatment.

Polarized Light Microscopy. Crystalline PPSU obtained from DMF and spherulites of PPSU formed in DMAc were observed with a polarized-light optical microscope (Leica DM LM, Leica

Microsystems, Wetzlar, Germany) to confirm the existence of crystalline regions. Likewise, the melting of the crystalline structure was optically investigated by using a heating stage THMS 600 (Linkam Scientific Instruments, Tadworth, UK) for the PLM. The samples were subsequently heated in increments of 10 K with a heating rate of 10 K/min up to 240 °C (solutions in DMAc) and 300 °C (solutions in DMF) and hold at each temperature step for 5 minutes. A slow cooling interval followed at a cooling rate of 0.1 K/min down to 25 °C to check if crystalline structures also form during cooling from the melt state.

Atomic Force Microscopy. A Bruker MultiMode 8, (Bruker Corporation, Santa Barbara, CA, USA), obtained the image of crystalline PPSU samples, in Peak Force QNM mode (qualitative nanomechanical mapping) as well as in tapping mode at room temperature (22-24 °C). ScanAsyst-Air probes (tip radius 2 nm, spring constant 0.4 N/m) were applied for Peak Force QNM. RTESPA-150 probes (tip radius 8 nm, spring constant 6 N/m) and high aspect ratio-probes TESP-SS (tip radius 2 nm, spring constant 20 – 80 N/m) were applied for tapping mode. Images with the highest accuracy were acquired using tapping mode with the high aspect ratio-TESP-SS probes due to the rough surface of the samples. All probes were purchased from Bruker, Massachusetts, USA. Images were processed with Nanoscope Analysis 1.9 regarding the removal of tilt with the plane-fit function, regarding the adjustment of contrast and brightness as well as for measurements of profiles of the crystalline lamellae.

Scanning Electron Microscopy. Further characterization of the surface of the samples was performed with a scanning electron microscope Merlin (Zeiss, Oberkochen, Germany). The secondary electron micrographs were taken with an acceleration voltage of 3-5 kV. For charge oppression, the samples were coated with a platinum layer of 2 nm thickness by a sputter coater Bal-tec MED 020 (Bal-tec/Leica Microsystems GmbH, Wetzlar, Germany).

Wide-Angle X-Ray Scattering. The crystallinity and the diffraction patterns were evaluated by wide-angle X-ray scattering measurements, using a flexibly convertible small/wide-angle X-ray scattering SAXS/WAXS device equipped with an Incoatec IμS X-ray source and Quazar Montel optics. A SX165 CCD-Detector (Rayonix L.L.C., Evanston, USA) recorded the patterns with a collection time of 600 s per WAXS measurement. The samples were measured in transmission. The sample-detector distance was 0.15 m, so a possible detection of an angular range of $2\Theta = 5°–45°$ was given. The spot size at the sample position was 700 μm and the X-rays wavelength was 0.154 nm. The analysis and reduction of X-ray data was carried out with the customizable software DPDAK[29]. The quantification of crystallinity χ_c was done by data analysis in Origin[30], according to Equation 1, after subtraction of instrumental background signals.

Equation 1

$$\chi_c = \frac{A_c}{A_c + A_a} \quad (1)$$

In Equation 1 A_c is the integrated area of the crystalline peaks and A_a the integrated area of the amorphous area.

Fourier Transform Infrared Spectroscopy. Fourier transform infrared (FTIR) spectra were recorded in attenuated total reflectance (ATR) mode with a Bruker ALPHA ATR FT-IR spectrometer (Bruker, Ettlingen, Germany), equipped with a diamond crystal. The measurements were carried out at ambient temperature in a spectral range of 400–4000 cm^{-1}. An average of 32 scans and a resolution of 4 cm^{-1} was applied for recording the spectra.

Differential Scanning Calorimetry. Differential scanning calorimetry was performed with a DSC 1 Star System (Mettler Toledo, Greifensee, Switzerland) and used to study the thermal

transitions in the temperature range from -100 °C to 320 °C in a nitrogen atmosphere. All DSC runs were carried out at a rate of 10 K/min. For evaluation of melting temperature, T_m, only the first heating scan was considered, and after the cooling interval where the thermal history has been erased, the third scan was analyzed to determine the glass transition temperature, T_g. The crystallinity in the cooling and the second heating interval could not be determined via DSC measurements, since the required resolution to display the crystallization enthalpy of an eventually very low crystalline proportion formed out of the melt was too high to be obtained in the DSC measurements. Therefore, only the enthalpy for the crystal melting, but not for crystallization was evaluated.

Nuclear Magnetic Resonance Spectroscopy. Samples were prepared with a concentration of 15 % in deuterated DMF. ^{1}H-NMR spectra were recorded using an Bruker Avance III HD 500 NMR spectrometer (Bruker, Rheinstetten, Germany) operating at a field of 11.7 Tesla (500.13 MHz) employing a 5 mm ^{1}H/^{13}C/^{15}N PATXI probe and a sample temperature of 25 °C. The spectra were recorded by employing the zg30 sequence using a 2.6 µs 30° pulse. The repetition time was set to 5 s to make sure that the samples were fully relaxed.

Rheology. A rotational rheometer MCR 502 (Anton Paar, Graz, Austria) was used for the investigations of the viscoelastic behaviour of the solutions in shear. For low viscous solutions a Searle geometry and for crystallized samples a plate-plate geometry was used for the rheological experiments. The measurements were performed at a temperature of 25 °C in a nitrogen atmosphere. For the frequency sweeps the shear amplitude was set to γ_0 = 10 %. The range of angular frequencies covered 100 to 0.01 rad s^{-1}.

RESULTS AND DISCUSSION. In this study, crystallization of poly(phenylene sulfone) in poor solvents was investigated. Rheological experiments revealed that PPSU, dissolved in NMP, DMAc or DMF is not stable for all solvents at ambient conditions, i.e. the viscoelastic behaviour changes with time. Figure 2 shows the magnitude of the complex viscosity $|\eta^*|$ for the three solutions as a function of the angular frequency ω. With time, the solutions of PPSU in DMF and DMAc develop a pronounced Non-Newtonian character with shear-thinning behaviour. This behaviour is caused

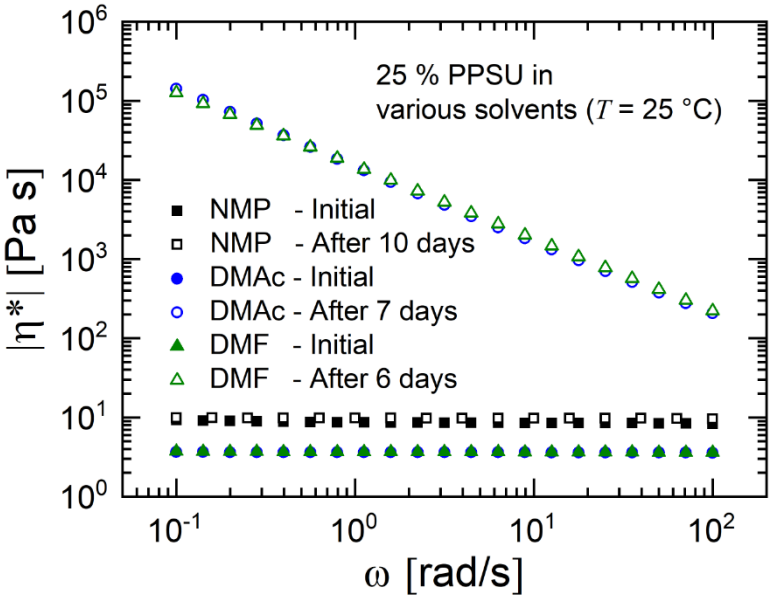

Figure 2. Evolution over time of the magnitude of complex viscosity as a function of the angular frequency for PPSU in NMP, DMF and DMAc.

by the increase of dynamic moduli and the non-Maxwell model type behaviour. However, PPSU in NMP remains an almost Newtonian solution, pointing that NMP is the best solvent for PPSU and no change of internal structure takes place. Cloud point measurements support these observations (Figure 3). Due to the ongoing crystallization in the poor solvents, the cloud points were determined for solutions of different concentrations (6, 9 and 12 % PPSU). That way it could

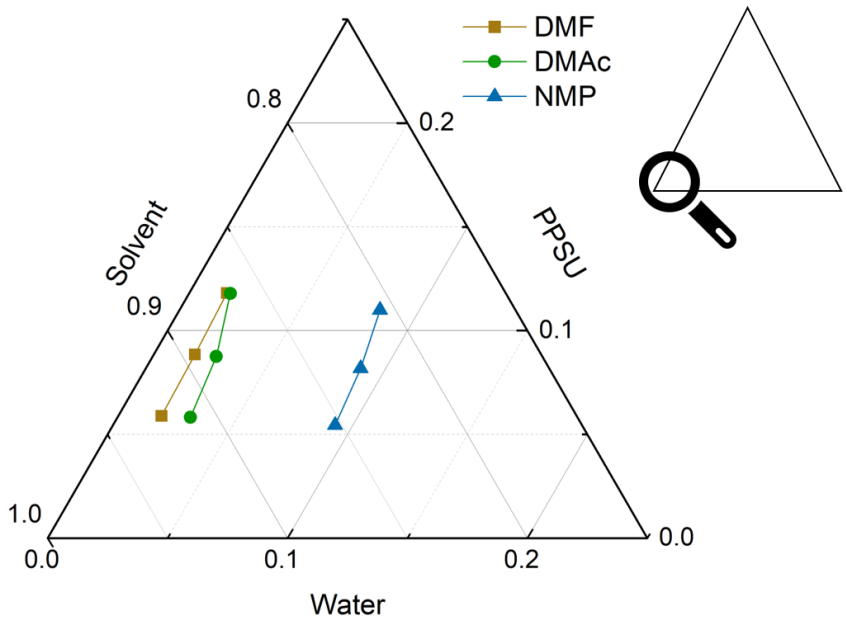

Figure 3. Cloud points of solutions of PPSU in DMF, DMAc and NMP.

be assured, that the cloud point was not reached due to the crystallization over time, but only due to the addition of non-solvent.

Morphology of Crystals. Figure 4 shows the development of solutions of 25 % PPSU in NMP, DMAc and DMF directly after preparation, after one and after four days. Obviously, the solution with NMP is stable. According to our investigations, it seems stable for at least six months at ambient conditions. The progression of crystallization at this concentration is visible by eye in both, DMAc and DMF, already after 24 h. The solution with 25 % PPSU in DMF is turbid almost immediately after mixing. At lower concentrations of 7 % the solution is transparent for some days before turning turbid. However, the spherulites in DMAc at a concentration of 7 % PPSU, grow

within two weeks instead of 24 h as it has been determined for 25 % solutions. The investigations

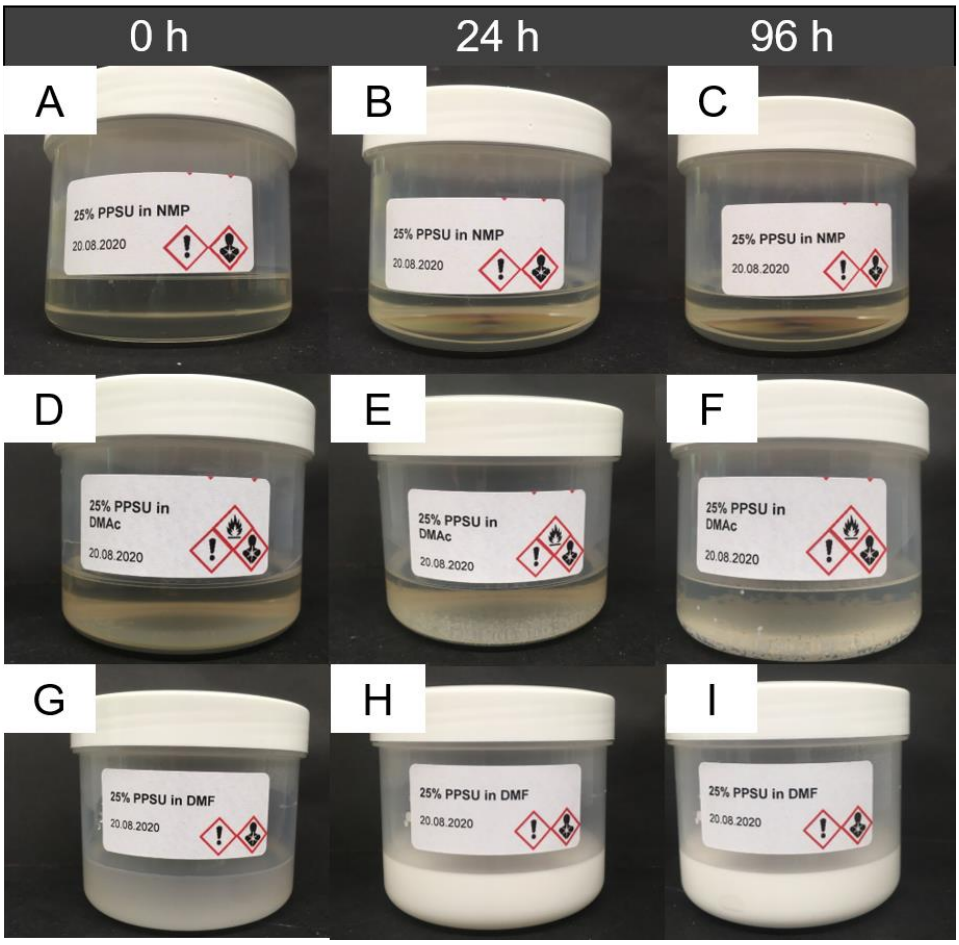

Figure 4. Photographs of solutions of 25% PPSU in NMP (A-C), 25% PPSU in DMAc (D-F) and 25% PPSU in DMF (G-I) at times of 0 h, 24 h and 96 h after preparation.

at various concentrations show that the concentration only influences the time scale of crystallization, but not if crystallization occurs at all (see supporting information). This implies that the origin of the crystallization process is not saturation, but solvent quality and interactions within the PPSU chains. For purposes of comparability and preferably fast crystallization processes, the authors choose to perform all following investigations on solutions with 25 % PPSU in the solvent of choice, or dried PPSU out of a 25 % solution. The melting temperature of the

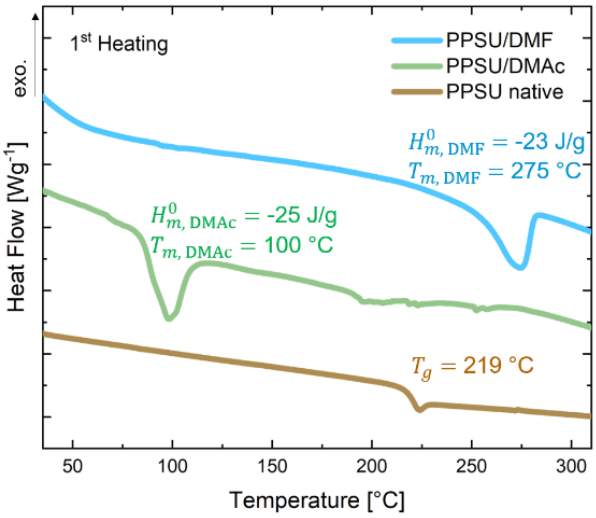

Figure 5. DSC thermograms revealing a T_g (first heating run) of 219 °C for native PPSU flakes and melting peaks at T_m = 100 °C for crystallized PPSU/DMAc and T_m = 275 °C for PPSU/DMF solutions.

crystalline regions was investigated via PLM and DSC on dried samples (60 °C for 14 days in vacuum). According to thermal gravimetric analysis (TGA) the samples after drying contained still 10 % (DMF) and 20 % (DMAc) of solvent captured in their structures (SI: TGA). The first heating run of the DSC thermograms is shown in Figure 5. Measurements on native PPSU flakes as delivered for comparison and dried PPSU in DMF and DMAc are displayed. Sample evaluation via FTIR[31-33] on crystallized PPSU in DMF and DMAc, compared with native PPSU and the pure solvents (Figure 6), could not detect any significant shifts in the signals in the polymer/solvent solutions. At wavenumbers in the range of 1760-1690 cm^{-1} the C=O stretching vibrations (a) are visible, while the signals at 1350-1030 cm^{-1} correspond to stretching N-C vibrations (b) which can be associated with the solvents. The C-O-C stretching vibration at 1225-1200 cm^{-1} as well as 1150-1060 and 970-800 cm^{-1} belong to the ether group (c), while the sulfone group of PPSU (d) absorbs with S=O stretching vibrations at 1350-1300 and 1160-1120 cm^{-1}. Distinct vibrations of the aromatic ring compounds are found at 1600, 1500 and a deformation at 1000 cm^{-1}. The vibrations

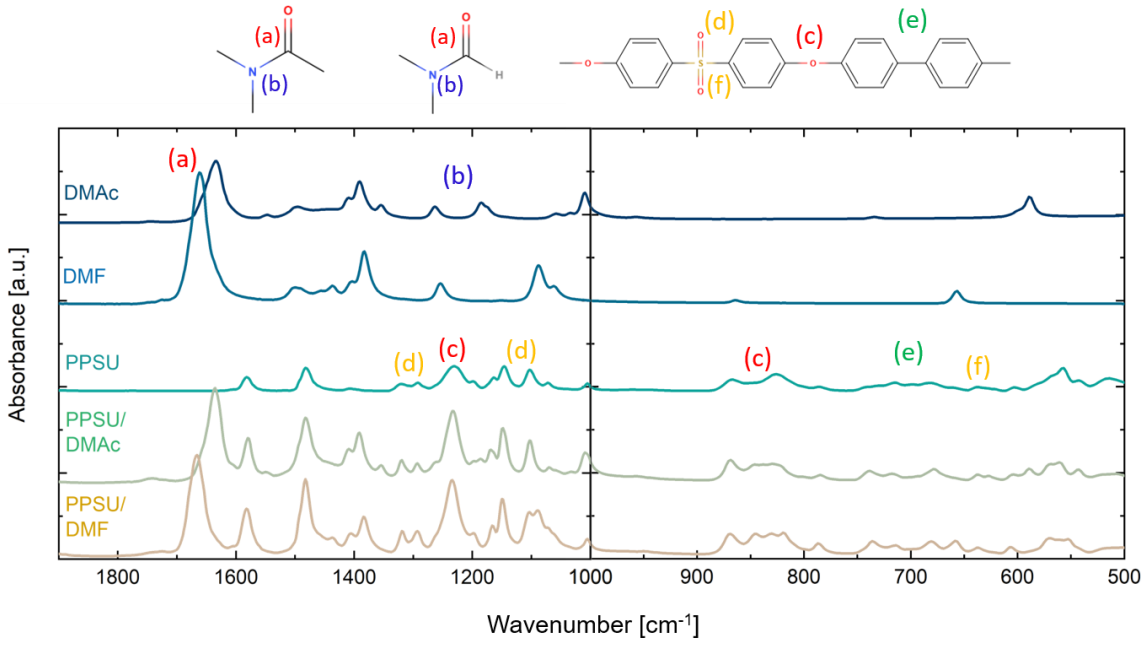

Figure 6. FTIR analysis of the crystalline samples and their components, exact peak positions can be found in the SI.

of the compound class C-S (f) can be found at 800-600 cm^{-1}. This region overlaps with the out of plane deformation of substituted benzene rings at 900-600 cm^{-1} (e). The absorption peak positions of the solution are in good agreement with those of the native materials. That might exclude binding effects of solvent molecules onto the polymer. Nonetheless, at wavenumbers from 900-600 cm^{-1}, the signals appear distinct and narrow for the solutions. This region covers both, the vibrations of the biphenyl group, as well as the substituted benzene rings on the sulfone, and the ether group. It seems that at least one of these compounds are particularly effected from crystallization. The aromatic rings are also represented in the signal at 1580 cm^{-1} (1600 cm^{-1}, according to literature[31]), which is more pronounced in the crystallized solutions. These results imply that the reason for crystallization is found in interactions of the polymer backbone and the solvent is only captured in the crystalline structure, but not covalently bonded.

The heating in the Linkam stage of the PLM was performed at a rate of 10 K/min and images were taken at intervals of 5 minutes at constant temperatures. A slow cooling rate of 0.1 K/min was chosen after melting of the samples in order to verify if crystallization can also occur directly from the melt (Figure 7). The values of T_m observed in both investigations, DSC and PLM, are in good agreement. The T_m of PPSU in DMF was measured to be 275 °C, with a T_g of native PPSU at 219 °C. This finding is in good agreement with the empirical rule of Beaman-Boyer[34-35], stating that the T_g correlates roughly with 2/3 T_m. However, the crystallized PPSU in DMAc revealed a surprisingly low melting temperature of the spherulites at 100 °C. The slow cooling of molten, native PPSU, did not result in measurable, reinduced crystallinity. Although slight lamellae formation could be observed in AFM images (see SI), the crystallinity of these samples was too

low to be measurable via DSC or WAXS. One could probably come to higher crystallinities by extending the duration of the PPSU being stored at a temperature above T_g.

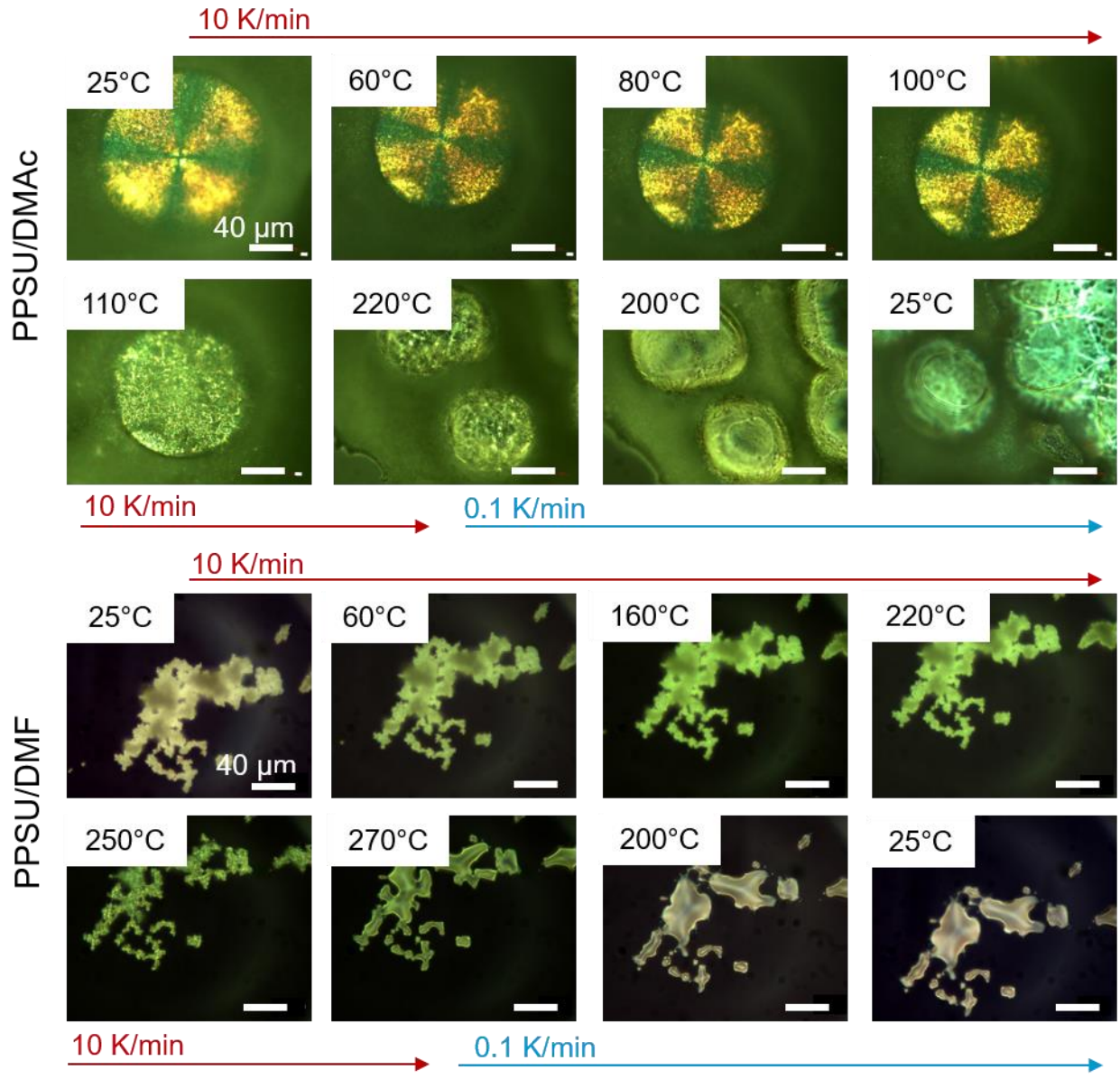

Figure 7. PLM images, taken at different temperatures for visualization of the melting of crystalline structures. For clear presentation, only selected temperatures are shown here. Melting temperatures were 100 °C and 270 °C for PPSU/DMAc and PPSU/DMF, respectively. A slow cooling interval with a rate of 0.1 K/min to examine if crystallization from the melt is possible followed the heating interval.

The morphology of those crystalline structures is depicted in Figure 8 and offers a possible explanation for the different melting temperatures. A less dense crystalline structure may cause a

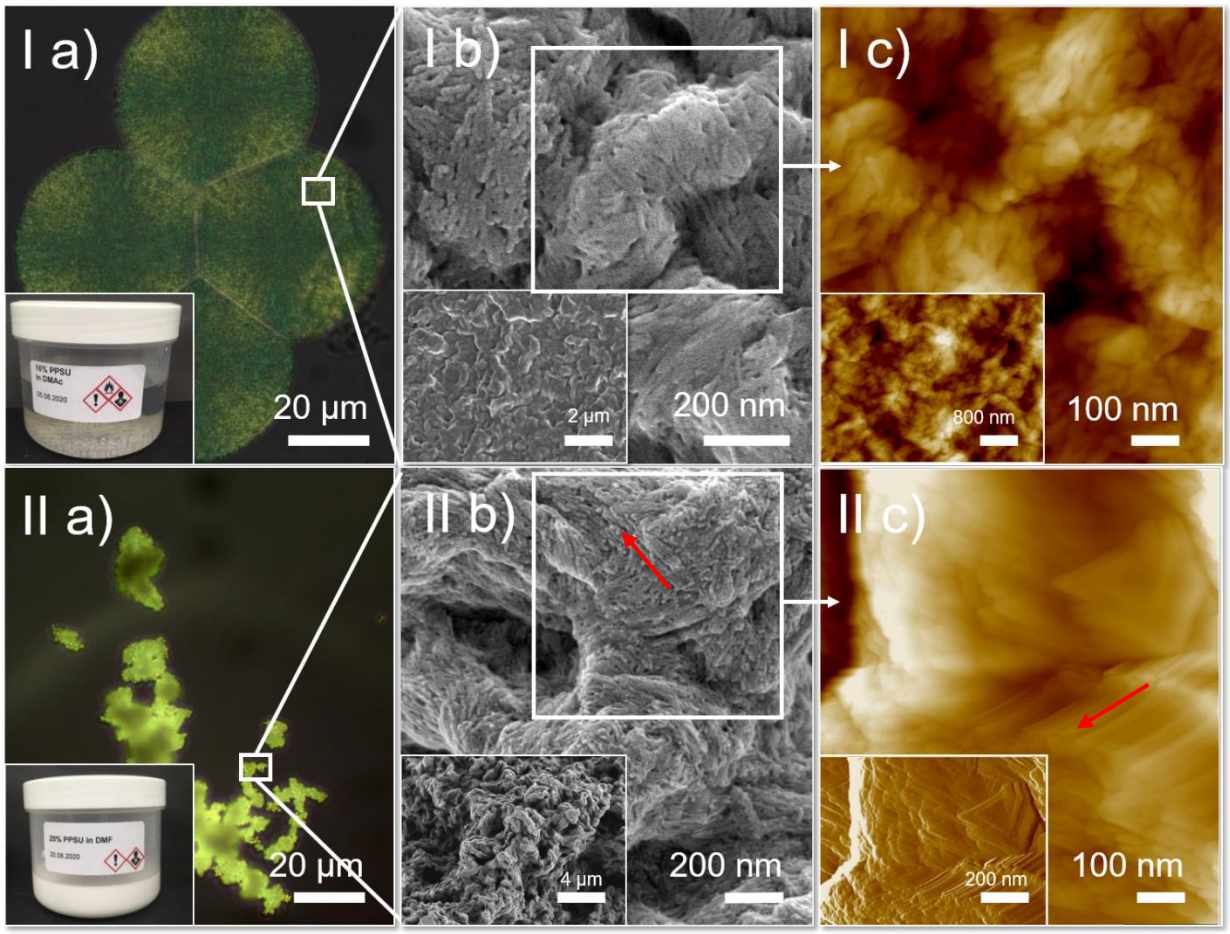

Figure 8. Morphology of crystallized PPSU from solutions with DMAc (I) and with DMF (II). Column a) shows PLM images, b) presents scanning electron micrographs and c) depicts the AFM height profiles of the sample from 0-165 nm dark to light, height profile of the inset I c) ranges from 0 to 330 nm. The inset in II c) gives the amplitude error of the AFM tip, providing a better visible morphology. Red arrows alert to the fibril orientation leading to plate-shaped structures.

low crystalline melting temperature of the spherulitic PPSU, compared with the PPSU crystals grown in DMF. The decreased ability of DMF to dissolve PPSU sufficiently, compared to DMAc (and NMP) has a similar effect like pressure-induced crystallization for polymers in the melt. The lower the quality of the solvent, the higher is the number of favorable interactions between adjacent chains in the melt. It is known that elevated pressure on crystallizable polymers in the molten state introduces more nuclei, involving a rise of melting temperature[36-37]. AFM investigations revealed

plate- and chair-shaped structures of 150 nm lateral expansion and 20 nm thickness (Figure 8, II c and inset). The plates consist of similar fibrils like the spherulites but seem to have a more ordered spatial orientation (Figure 8, I and II b)). The fibrils have a constant thickness of 10 nm ± 2 nm and 75 nm ± 10 nm in length, as determined by analysis of the scanning electron micrographs. The low melting temperature of the spherulites suggests a rather imperfect crystallization through incorporation of solvent molecules. Although a typical, distinct maltese cross, including the rings known from banded spherulites, is visible in the images from polarization microscopy (Figure 8, I a), there were no branched or star-like orientated substructures visible via SEM or AFM, as expected from literature for typical spherulite growth[38-41]. This could be an indication for defects in the crystal or elevated mobility through captured solvent molecules in the crystalline structure, as has been found before by several researchers investigating crystals with low melting temperatures[42-43]. If these assumptions are true, one could expect the number of defects to be even more pronounced in the samples crystallized from DMF. For PPSU in DMF a full incorporation of the solvent molecules into the crystalline structure was observed. Following the above-mentioned approach, this should lead to even more defects compared with the imperfect, but still well established spherulites. An explanation could describe defect-free grown crystals in parts of the mixture, where the chain-chain interaction is high and the distances of interacting molecules are very low. These crystalline parts can be accompanied by pronounced interconnection through amorphous parts, where the solvent molecules are captured and integrated. That would lead to a 3D dispersion with dense crystalline packing but macroscopically homogeneous appearance. In

addition, the defect-free, densely packed crystals would feature a higher melting temperature as found in the DSC and PLM investigations.

Crystallinity. The crystallinity was determined, using wide-angle X-ray scattering (WAXS). Lacking knowledge of the crystal unit cell of PPSU itself, only the periodic line patterns, the associated *d*-spacing, as well as the crystallinity are evaluated. The observed scattering peak positions are reported in Figure 9 and Table 1.

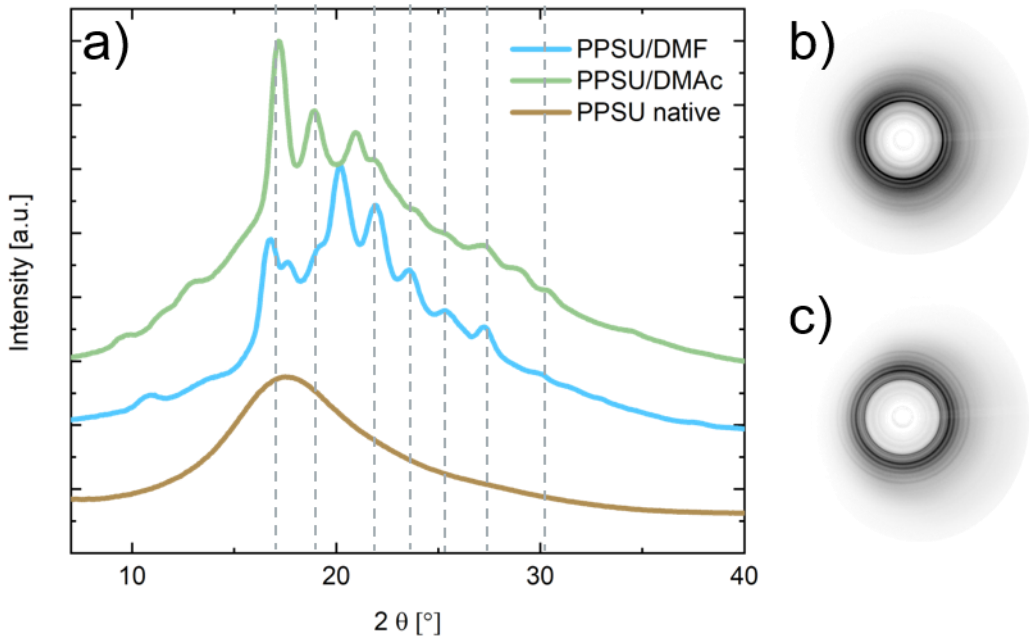

Figure 9. WAXS scattering intensity diagram of native PPSU flakes (amorphous, brown) and dried PPSU/DMF (blue) as well as PPSU/DMAc (green). The dashed lines indicate peak positions, shared in both samples. The exact values of all peak positions are listed in Table 1. b) and c) depict the WAXS intensity of PPSU/DMAc and in DMF, respectively. Distinct radial positions indicate the reflections of the crystal and are visible in the amorphous halo.

Table 1. Crystalline reflections of dried PPSU crystals, grown in solutions with DMAc and DMF, obtained by WAXS measurements.

2θ (°)	**16.9**	**17.8**	**18.7**	**20.1**	**21.0°**	**22.0**	**24.0**	**25.1**	**28.3**	**29.2**	**30.3**
PPSU/DMAc	x		x		x	x	x	x	x	x	x

PPSU/DMF x x x x x x x x x

The *d*-spacing correlates to Bragg's law (Equation 2), with an X-ray wavelength of 1.54 Å and the order of diffraction *n*. With $n = 1$, the values for the lattice spacing could be calculated, see

The most prominent distance was calculated to be close to 5.3 Å for both crystalline structures. However, it was not possible to match the *d*-spacings to their corresponding lattice planes without the unit cell parameters.

Table 2.

Equation 2.

$$n\lambda = 2d \sin\theta$$

The most prominent distance was calculated to be close to 5.3 Å for both crystalline structures. However, it was not possible to match the *d*-spacings to their corresponding lattice planes without the unit cell parameters.

Table 2. Calculated *d*-spacing for the three most pronounced peaks of PPSU in DMAc or DMF.

2Θ [°]		*d*-spacing [Å]	
DMAc	DMF	DMAc	DMF
16.90	16.72	5.24	5.30
18.66	20.10	4.74	4.41
21.04	21.95	4.21	4.04

The crystallinity for both samples was calculated using Equation 1. For PPSU/DMAc the calculated crystallinity was 37 % and for PPSU/DMF 50 %.

These values are in good agreement with all observations above. The elevated crystallization kinetics may result from a combination of more nuclei and another crystalline form. The crystalline growth in DMF was tracked and the development of crystallinity plotted over time, see Figure 10. Note, that the calculated crystallinity for 25 % PPSU in DMF is obviously much lower, compared to a dried sample. For the calculations, the normalized scattering data at 0 h were chosen for the amorphous state. The data reveal an exponential increase of crystallinity probably due to a high nucleation number, as explained before. The stationary number of nuclei, introduced by the solvent quality of DMF, governs the unhindered crystallization in the first 60 hours. Afterwards the growth of the crystals must be spatially hindered, as also observed in the solutions texture, which showed higher dynamic moduli after 60 h, see rheological measurements in the SI. The crystallinity converges to a constant value of 14 %. If one considers that only the polymer chains crystallize, 14 % crystallinity of a solution with 25 % polymer in solution corresponds to 56 % crystallization of the homopolymer. This is in good agreement with the calculations above.

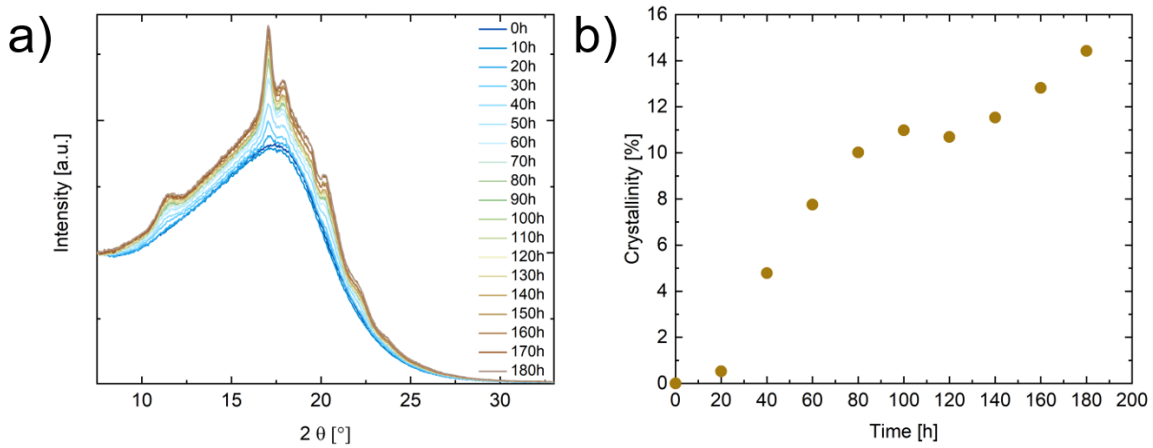

Figure 10. Progression of crystalline formation over time for 25 % PPSU in DMF, obtained via WAXS measurements. a) Shows growth of scattering intensity, in b) calculated crystallinity in solution as function of time.

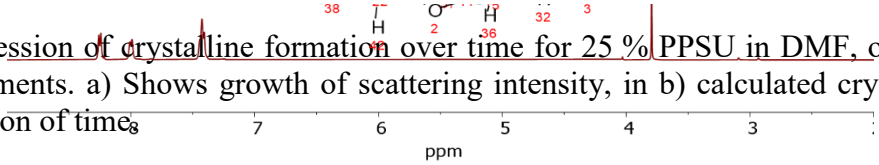

Figure 11. ^{1}H NMR spectra of PPSU. Top: Calculated; Bottom: Measured spectrum.

For PPSU in DMAc the attempt to track the increase of crystallinity over time was not successful. This may be the case because the crystallinity is lower and slowly increasing, but more important was that the nucleation happened mostly on surfaces due to their roughness/defects and when the crystallization in the solution started, the spherulites sank to the bottom of the specimen and the detection of the crystallites was not possible. The same effect was seen in the ^{1}H NMR measurements. For clear identification, the predicted and measured spectra of PPSU are displayed in Figure 11. Note, that the simulation of only one repeating unit for the calculated PPSU spectrum is not realistic for an apparent number average molecular mass of 26 kDa, so the predicted peak intensity of the endgroup at δ3.8 ppm is too high. Here, water is the reason why the measured spectrum still shows a well-pronounced peak at δ3.8 ppm, as the solution is highly hygroscopic. A detailed peak identification can be found in the SI. With time, broadening of the corresponding peaks for the conjugated systems in PPSU was visible in DMF, agglomeration together with π–π stacking[44-45] could explain this phenomenon, see Figure 12. Especially, in the aromatic region for

the biphenyl group (7.8-8.4 ppm), the slight chemical shift to higher frequencies as well as the broadening of the multiplet peaks point to interacting molecules in solution. π-π–stacking interactions of the biphenylene unit contribute to evoking the aromatic ring current effect, which

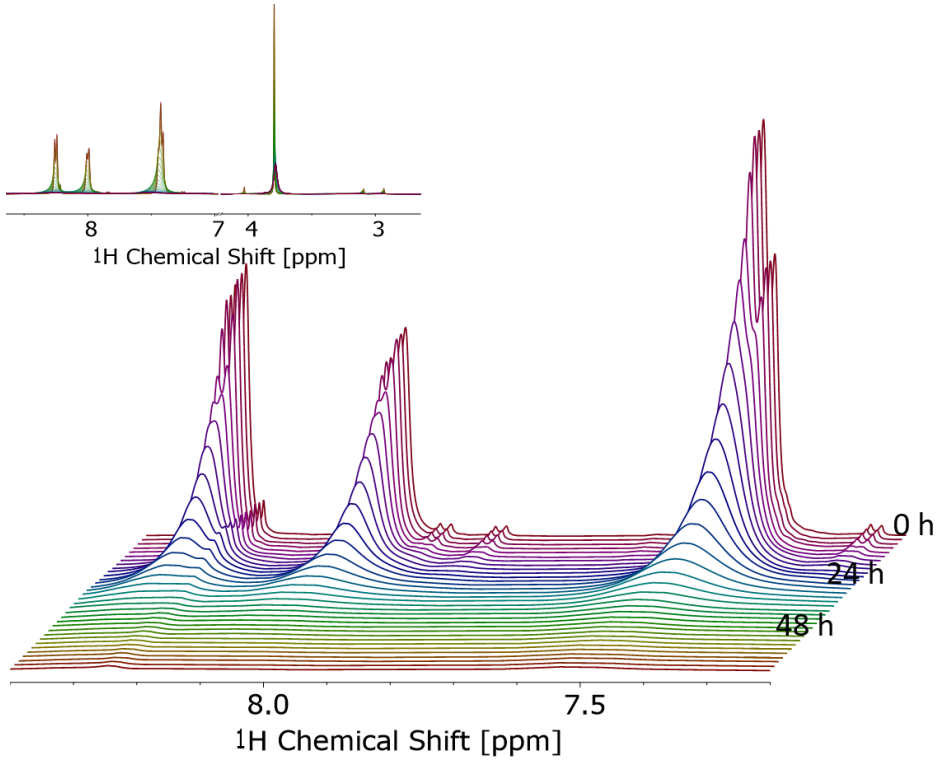

Figure 12. Enlarged aromatic region of the stacked ^{1}H NMR spectra of PPSU in DMF, measured for 64 h. The inset shows the complete superimposed series.

leads to a deshielding of the protons and a downfield shift of the signals. The diminished mobility of the growing crystals in the solution, results in broadening of the signals[46-48].

For PPSU in DMAc, this downfield shift could not be measured, not because crystallization did not occur, but the spherulites show a higher density than the solution and sink to the bottom of the NMR tube.

Instead, the crystalline growth of PPSU in DMAc could only be tracked via optical microscopy, as it is shown in Figure 13. A slightly different trend accounts for the spherulitic growth, compared to the crystallization of PPSU in DMF (Figure 10) over time. Due to the better solvent

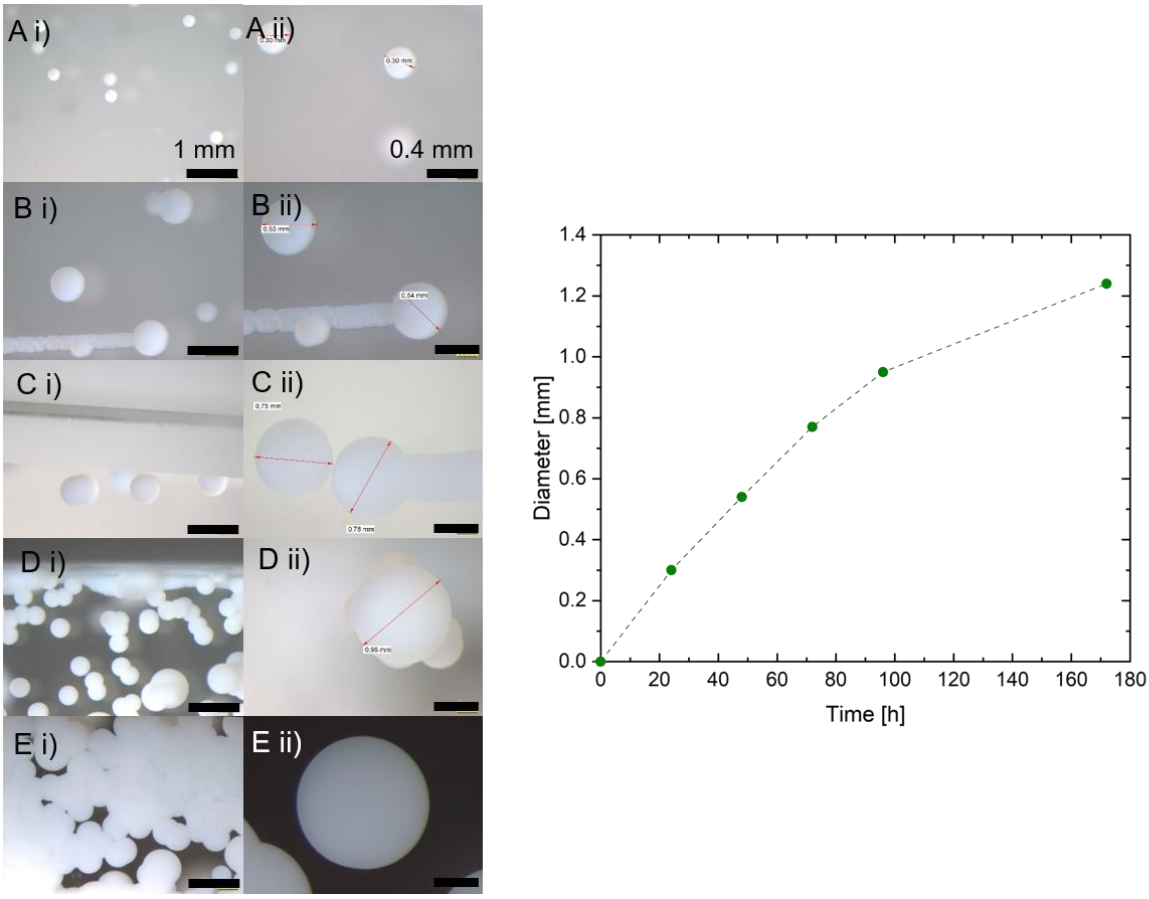

Figure 13. Spherulitic growth of 25% PPSU in DMAc over time. Images A-E were taken via light microscopy.

quality, the number of nuclei must be smaller, resulting in more three-dimensional space for crystal growth. Nevertheless, the growth of the spherulites almost follows a linear increase, until the boundary of other spherulites is reached after 160 h and the growth no longer takes place in the lateral dimension, but new spherulites on the first generation will be formed.

CONCLUSION. This study investigated two mechanisms of crystallization of commonly known amorphous PPSU in poor solvents. It was shown that crystallinity in a bad solvent (DMF) is enhanced, compared to better solvents (DMAc and NMP), leading to different melting temperatures and different crystalline forms. The driving force for the crystallization itself might be π–π stacking of the biphenylene groups, which was supported by the NMR spectra of PPSU in

DMF. Estimated lamellar distances could be determined via AFM and corresponding scanning electron micrographs with a lamellar thickness of 10 nm, while the atomic plane distances range from 4.2 to 5.3 Å, as has been calculated from WAXS data.

ASSOCIATED CONTENT

Supporting Information. The following files are available free of charge. Additional SEM and AFM micrographs, AFM height profiles, AFM images of crystallized PPSU from melt, TGA data, dynamic moduli as determined by rheological investigations, photographs of low concentrated solutions (7 %) of crystallized PPSU in DMAc and DMF after 30-days, full FTIR spectra, table of FTIR absorption and according compound classes, additional NMR data for peak identification (PDF).

AUTHOR INFORMATION

Corresponding Author

*ulrich.handge@hzg.de;Tel.: +49 4152 87 2446, Helmholtz-Zentrum Geesthacht, Institute of Membrane Research, Max-Planck-Strasse 1, 21502 Geesthacht, Germany

Author Contributions

The manuscript was written through contributions of all authors. All authors have given approval to the final version of the manuscript.

Funding Sources

This work is financially supported by the BMBF project MABMEM, grant no. 03XP0043E.

ACKNOWLEDGMENT

The authors thank Ivonne Ternes (rheology, DSC), Hermann Kriegel (XRD), Evgeni Sperling (AFM), Dr. Martin Held, Anke-Lisa Höhme and Dr. Erik Schneider (SEM), Silvio Neumann (NMR, TGA), Petra Merten (GPC) and in particular Joachim Koll for experimental support and scientific discussions. Special thanks go to the BMBF who financially supported this project (03XP0043E) and the BASF SE who kindly provided the investigated polymer batches.

ABBREVIATIONS

AFM, atomic force microscopy; DMAc, *N,N´*-dimethylacetamide; DMF, *N,N´*-dimethylformamide; DSC, differential scanning calorimetry; FTIR, Fourier transform infrared spectroscopy; NMP, *N*-methyl-2-pyrrolidone; NMR, nuclear magnetic resonance spectroscopy; PLM, polarized light microscopy; PPSU, poly (phenylene sulfone); SEM, scanning electron microscopy; SI, supporting information; WAXS, wide angle X-ray scattering.

REFERENCES

1. Guo, H.; Nicolae, A.; Kumar, V., Fabrication of high temperature polyphenylsulfone nanofoams using high pressure liquid carbon dioxide. *Cellular Polymers* **2016,** *35* (3), 119-142.
2. Sun, H.; Sur, G. S.; Mark, J. E., Microcellular foams from polyethersulfone and polyphenylsulfone: Preparation and mechanical properties. *European Polymer Journal* **2002,** *38* (12), 2373-2381.
3. Slonov, A. L.; Khashirov, A. A.; Zhansitov, A. A.; Rzhevskaya, E. V.; Khashirova, S. Y., The influence of the 3D-printing technology on the physical and mechanical properties of polyphenylene sulfone. *Rapid Prototyping Journal* **2018**.
4. Eckardt, M.; Greb, A.; Simat, T. J., Polyphenylsulfone (PPSU) for baby bottles: a comprehensive assessment on polymer-related non-intentionally added substances (NIAS). *Food Additives & Contaminants: Part A* **2018,** *35* (7), 1421-1437.
5. Gronwald, O.; Frost, I.; Ulbricht, M.; Kouchaki Shalmani, A.; Panglisch, S.; Grünig, L.; Handge, U. A.; Abetz, V.; Heijnen, M.; Weber, M., Hydrophilic poly(phenylene sulfone) membranes for ultrafiltration. *Separation and Purification Technology* **2020,** *250*, 117107-117117.
6. Panglisch, S.; Kouchaki Shalmani, A.; Weber, M.; Gronwald, O.; Berg, P.; Heijnen, M.; Krug, M.; Koti, M.; Nahrstedt, A.; Abetz, V.; Handge, U. A.; Grünig, L.; Ulbricht, M.; Stratmann, I., Material Selection Box for the Production of Advanced Polymer Membranes for Water Treatment. *Chemie Ingenieur Technik* **2019,** *91* (8), 1162-1167.
7. Dai, J.; Li, S.; Liu, J.; He, J.; Li, J.; Wang, L.; Lei, J., Fabrication and characterization of a defect-free mixed matrix membrane by facile mixing PPSU with ZIF-8 core–shell microspheres for solvent-resistant nanofiltration. *Journal of Membrane Science* **2019,** *589*, 117261.
8. Feng, Y.; Han, G.; Chung, T.-S.; Weber, M.; Widjojo, N.; Maletzko, C., Effects of polyethylene glycol on membrane formation and properties of hydrophilic sulfonated polyphenylenesulfone (sPPSU) membranes. *Journal of Membrane Science* **2017,** *531*, 27-35.
9. Isloor, A. M.; Nayak, M. C.; Prabhu, B.; Ismail, N.; Ismail, A.; Asiri, A. M., Novel polyphenylsulfone (PPSU)/nano tin oxide (SnO2) mixed matrix ultrafiltration hollow fiber membranes: Fabrication, characterization and toxic dyes removal from aqueous solutions. *Reactive and Functional Polymers* **2019,** *139*, 170-180.
10. Liu, J.; Zhong, Z.; Ma, R.; Zhang, W.; Li, J., Development of High-Antifouling PPSU Ultrafiltration Membrane by Using Compound Additives: Preparation, Morphologies, and Filtration Resistant Properties. *Membranes* **2016,** *6* (2), 35.
11. Vijesh, A.; Krishnan, P. A.; Isloor, A. M.; Shyma, P., Fabrication of PPSU/PANI hollow fiber membranes for humic acid removal. *Materials Today: Proceedings* **2020**.
12. Shukla, A. K.; Alam, J.; Alhoshan, M.; Dass, L. A.; Ali, F. A. A.; Mishra, U.; Ansari, M. A., Removal of heavy metal ions using a carboxylated graphene oxide-incorporated polyphenylsulfone nanofiltration membrane. *Environmental Science: Water Research & Technology* **2018,** *4* (3), 438-448.
13. Decker, B.; Hartmann-Thompson, C.; Carver, P. I.; Keinath, S. E.; Santurri, P. R., Multilayer sulfonated polyhedral oligosilsesquioxane (S-POSS)-sulfonated polyphenylsulfone (S-PPSU) composite proton exchange membranes. *Chemistry of Materials* **2010,** *22* (3), 942-948.

14. Park, A. M.; Turley, F. E.; Wycisk, R. J.; Pintauro, P. N., Electrospun and cross-linked nanofiber composite anion exchange membranes. *Macromolecules* **2014,** *47* (1), 227-235.
15. Naderi, A.; Chung, T.-S.; Weber, M.; Maletzko, C., High performance dual-layer hollow fiber membrane of sulfonated polyphenylsulfone/Polybenzimidazole for hydrogen purification. *Journal of Membrane Science* **2019,** *591*, 117292.
16. Naderi, A.; Tashvigh, A. A.; Chung, T.-S.; Weber, M.; Maletzko, C., Molecular design of double crosslinked sulfonated polyphenylsulfone/polybenzimidazole blend membranes for an efficient hydrogen purification. *Journal of Membrane Science* **2018,** *563*, 726-733.
17. Colquhoun, H. M., Crystal and molecular simulation of poly (1, 4-phenylenesulfone). *Polymer* **1997,** *38* (4), 991-994.
18. Robello, D. R.; Ulman, A.; Urankar, E. J., Poly (p-phenylene sulfone). *Macromolecules* **1993,** *26* (25), 6718-6721.
19. Jurga, J., Crystal structure of poly (p-phenylene sulfide) by nuclear magnetic resonance spectroscopy. *Polymer* **1993,** *34* (20), 4203-4207.
20. Tabor, B.; Magre, E.; Boon, J., The crystal structure of poly-p-phenylene sulphide. *European Polymer Journal* **1971,** *7* (8), 1127-1133.
21. Feng, Y.; Han, G.; Zhang, L.; Chen, S.-B.; Chung, T.-S.; Weber, M.; Staudt, C.; Maletzko, C., Rheology and phase inversion behavior of polyphenylenesulfone (PPSU) and sulfonated PPSU for membrane formation. *Polymer* **2016,** *99*, 72-82.
22. Xu, Y. M.; Tang, Y. P.; Chung, T.-S.; Weber, M.; Maletzko, C., Polyarylether membranes for dehydration of ethanol and methanol via pervaporation. *Separation and Purification Technology* **2018,** *193*, 165-174.
23. Blackadder, D.; Ghavamikia, H.; Windle, A., Evidence for Crystallinity in Poly (ether sulphone). *Polymer* **1979,** *20* (June), 781-782.
24. Benhalima, A.; Hudon, F.; Koulibaly, F.; Tessier, C.; Brisson, J., Polyethersulfone polymers and oligomers - Morphology and crystallization. *Canadian Journal of Chemistry* **2012,** *90* (10), 880-890.
25. Wienk, I.; Boom, R.; Beerlage, M.; Bulte, A.; Smolders, C.; Strathmann, H., Recent advances in the formation of phase inversion membranes made from amorphous or semi-crystalline polymers. *Journal of Membrane Science* **1996,** *113* (2), 361-371.
26. Colquhoun, H. M.; Williams, D. J., Crystal and molecular simulation of high-performance polymers. *Accounts of Chemical Research* **2000,** *33* (3), 189-198.
27. Samitsu, S., Thermally stable mesoporous poly (ether sulfone) monoliths with nanofiber network structures. *Macromolecules* **2018,** *51* (1), 151-160.
28. Darvishmanesh, S.; Tasselli, F.; Jansen, J. C.; Tocci, E.; Bazzarelli, F.; Bernardo, P.; Luis, P.; Degrève, J.; Drioli, E.; Van der Bruggen, B., Preparation of solvent stable polyphenylsulfone hollow fiber nanofiltration membranes. *Journal of Membrane Science* **2011,** *384* (1-2), 89-96.
29. Benecke, G.; Wagermaier, W.; Li, C.; Schwartzkopf, M.; Flucke, G.; Hoerth, R.; Zizak, I.; Burghammer, M.; Metwalli, E.; Müller-Buschbaum, P., A customizable software for fast reduction and analysis of large X-ray scattering data sets: applications of the new DPDAK package to small-angle X-ray scattering and grazing-incidence small-angle X-ray scattering. *Journal of Applied Crystallography* **2014,** *47* (5), 1797-1803.
30. Corporation, O. *OriginPro2020*, 2020; 2020.
31. Weidlein, J.; Müller, U.; Dehnicke, K., *Schwingungsspektroskopie: Eine Einführung*. Thieme: 1982.

32. Zerbi, G.; Sandroni, S., Fundamental frequencies and molecular configuration of biphenyl—I. Re-analysis of its vibrational spectrum. *Spectrochimica Acta Part A: Molecular Spectroscopy* **1968,** *24* (5), 483-510.
33. Vojta, D.; Vazdar, M., The study of hydrogen bonding and π-π interactions in phenol ethynylbenzene complex by IR spectroscopy. *Spectrochimica Acta Part A: Molecular and Biomolecular Spectroscopy* **2014,** *132*, 6-14.
34. Beaman, R. G., Relation between (apparent) second-order transition temperature and melting point. *Journal of Polymer Science* **1952,** *9* (5), 470-472.
35. Boyer, R. F., Relationship of first-to second-order transition temperatures for crystalline high polymers. *Journal of Applied Physics* **1954,** *25* (7), 825-829.
36. Stamhuis, J.; Pennings, A., Crystallization of polyamides under elevated pressure: 6. Pressure-induced crystallization from the melt and annealing of folded-chain crystals of nylon-12, polylaurolactam under pressure. *Polymer* **1977,** *18* (7), 667-674.
37. van Drongelen, M.; van Erp, T.; Peters, G., Quantification of non-isothermal, multi-phase crystallization of isotactic polypropylene: The influence of cooling rate and pressure. *Polymer* **2012,** *53* (21), 4758-4769.
38. Bassett, D.; Olley, R., On the lamellar morphology of isotactic polypropylene spherulites. *Polymer* **1984,** *25* (7), 935-943.
39. Gránásy, L.; Pusztai, T.; Tegze, G.; Warren, J. A.; Douglas, J. F., Growth and form of spherulites. *Physical Review E* **2005,** *72* (1), 011605.
40. Hutter, J. L.; Bechhoefer, J., Banded spherulitic growth in a liquid crystal. *Journal of Crystal Growth* **2000,** *217* (3), 332-343.
41. Keith, H.; Padden Jr, F., A phenomenological theory of spherulitic crystallization. *Journal of Applied Physics* **1963,** *34* (8), 2409-2421.
42. Keith, H.; Padden Jr, F., Spherulitic crystallization from the melt. I. Fractionation and impurity segregation and their influence on crystalline morphology. *Journal of Applied Physics* **1964,** *35* (4), 1270-1285.
43. Fakirov, S.; Cagiao, M.; Baltá Calleja, F.; Sapundjieva, D.; Vassileva, E., Melting of gelatin crystals below glass transition temperature: a direct crystal-glass transition as revealed by microhardness. *International Journal of Polymeric Materials* **1999,** *43* (3-4), 195-206.
44. Parenti, F.; Tassinari, F.; Libertini, E.; Lanzi, M.; Mucci, A., π-Stacking signature in NMR solution spectra of thiophene-based conjugated polymers. *ACS Omega* **2017,** *2* (9), 5775-5784.
45. Platzer, G.; Mayer, M.; Beier, A.; Brüschweiler, S.; Fuchs, J. E.; Engelhardt, H.; Geist, L.; Bader, G.; Schörghuber, J.; Lichtenecker, R., PI by NMR: Probing CH–π Interactions in Protein–Ligand Complexes by NMR Spectroscopy. *Angewandte Chemie International Edition* **2020,** *59* (35), 14861-14868.
46. Dudenko, D.; Kiersnowski, A.; Shu, J.; Pisula, W.; Sebastiani, D.; Spiess, H. W.; Hansen, M. R., A Strategy for Revealing the Packing in Semicrystalline Π-Conjugated Polymers: Crystal Structure of Bulk Poly-3-Hexyl-Thiophene (P3HT). *Angewandte Chemie* **2012,** *124* (44), 11230-11234.
47. Fechtenkötter, A.; Saalwächter, K.; Harbison, M. A.; Müllen, K.; Spiess, H. W., Highly Ordered Columnar Structures from Hexa-peri-hexabenzocoronenes—Synthesis, X-ray Diffraction, and Solid-State Heteronuclear Multiple-Quantum NMR Investigations. *Angewandte Chemie International Edition* **1999,** *38* (20), 3039-3042.

48. Nandy, R.; Subramoni, M.; Varghese, B.; Sankararaman, S., Intramolecular π-stacking interaction in a rigid molecular hinge substituted with 1-(pyrenylethynyl) units. *The Journal of Organic Chemistry* **2007,** *72* (3), 938-944.

Figure SI 1. Photographs of 7 % PPSU in DMAc and in DMF, 4 weeks after preparation.

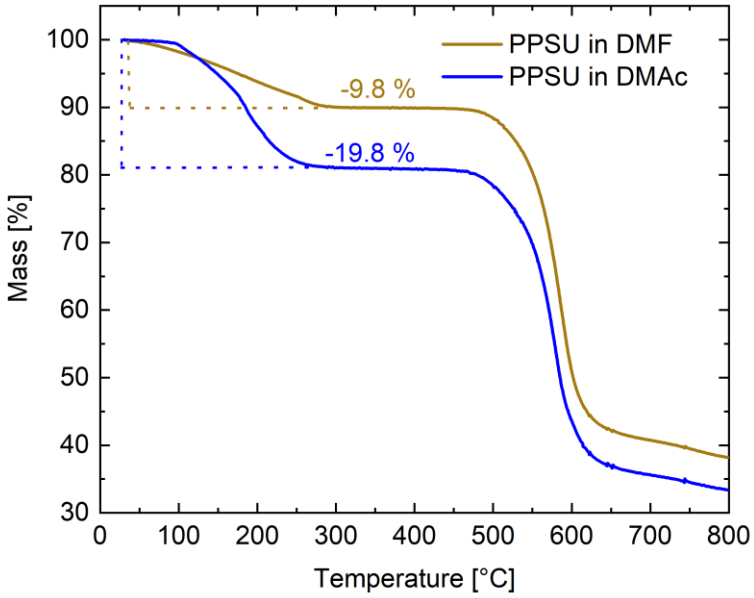

Figure SI 2. Thermogravimetric analysis of crystallized PPSU from DMAc and DMF, dried for 7 days at 70 °C under vacuum.

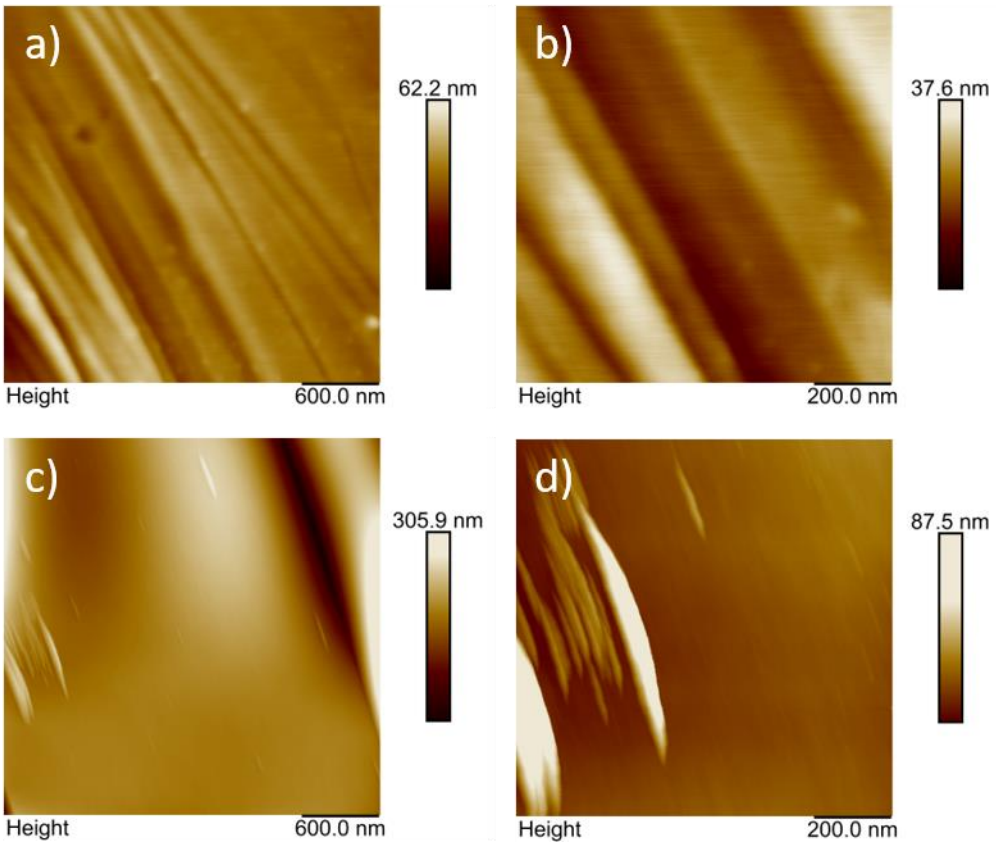

Figure SI 3. AFM micrographs of native PPSU, molten for 60 h at 240°C. After 60 hours a+b) were subsequently cooled with 10 K per hour, c+d) cooled down directly at 25°C.

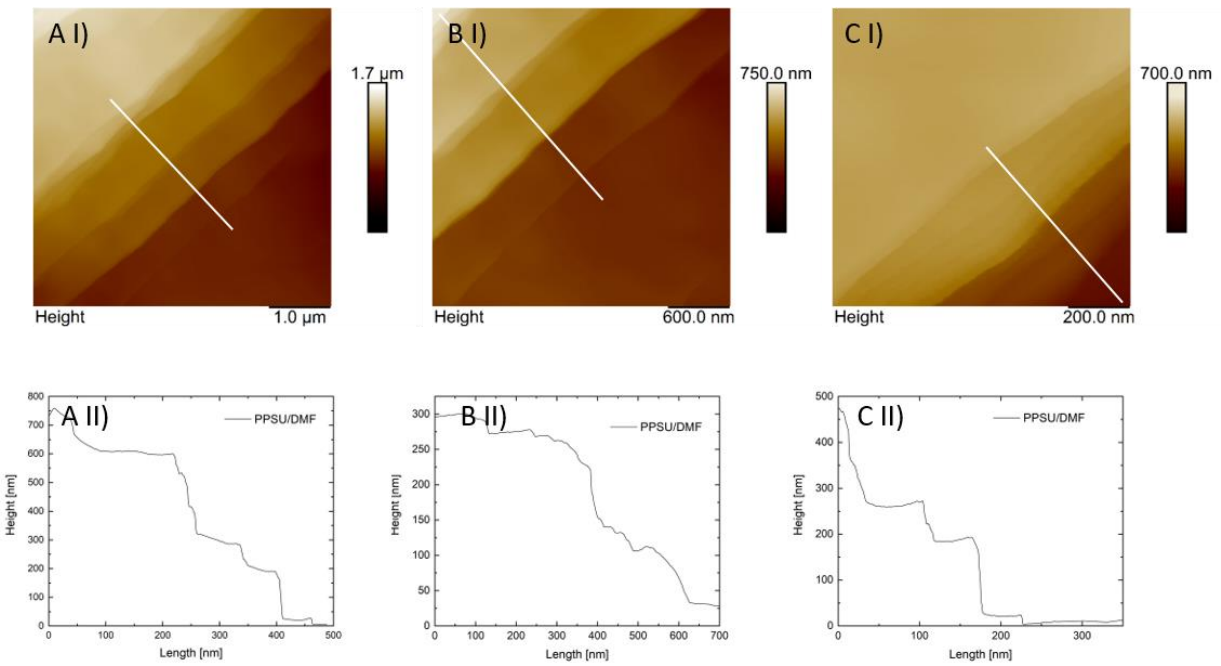

Figure SI 4. AFM micrographs (I) and height profiles (II) of PPSU plates, crystallized in DMF. The scanned area of the sample for was 5, 3 and 1 µm for A to C.

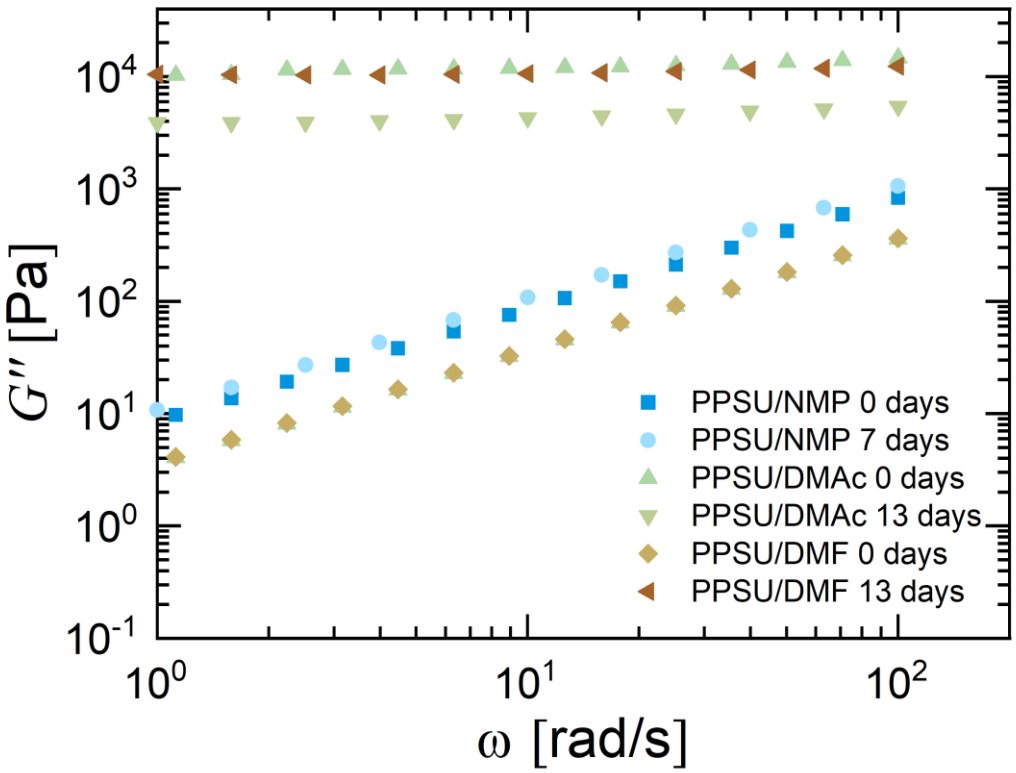

Figure SI 5. Loss modulus as a function of angular frequency ω for 25 %PPSU in NMP, DMAc and DMF directly after preparation and after seven (NMP) and 13 days (DMAc and DMF).

Table SI 1. Absorption peaks and according compound classes, determined by FTIR measurements.

Group	Absorption [cm^{-1}]	Absorption in spectra [cm^{-1}]				
		DMAc	DMF	PPSU	PPSU/DMAc	PPSU/DMF
$\nu_{CH2/3}$	3000-2800	2928	2926, 2852		2928	2926, 2852
$\nu_{C=O}$	1675-1630	1635	1661	0	1637	1665
$\nu_{C=C\ (ring)}$	1600, 1500	0	0	1582, 1482	1580, 1482	1582, 1482
$\delta_{C=C\ (ring)}$	1000			1003	1009	1005
ν_{C-N}	1360-1030	1353, 1264, 1184	1251, 1086, 1060		1353, 1252, 1186	1253, 1192, 1088
$\nu_{S=O}^{as}$	1350-1300			1319, 1292	1319, 1292	1317, 1294

$\nu^{s}_{S=O}$	1160-1120	1145*	1168, 1147*	1166, 1150*
ν_{C-O}	1225-1200	1229	1231	1233
ν^{as}_{C-O-C}	1150-1060	1145*, 1103, 1072	1147*, 1103, 1070	1150*, 1103, 1088
ν^{s}_{C-O-C}	970-800	866*, 825*	868*, 848-825*	872*, 843-819*
ν_{C-S}	800-600	717*, 683*	715*, 679*	787*, 683*
γ_{C-H} (o.o.p. subst. benzene)	900-670	866*, 825*, 717*, 683*	868*, 848-825*, 785*, 736*, 715*, 679*	872*, 843-819*, 787*, 734*, 713*, 683*

*Absorption peaks are ambiguous and therefore listed in multiple compound classes.

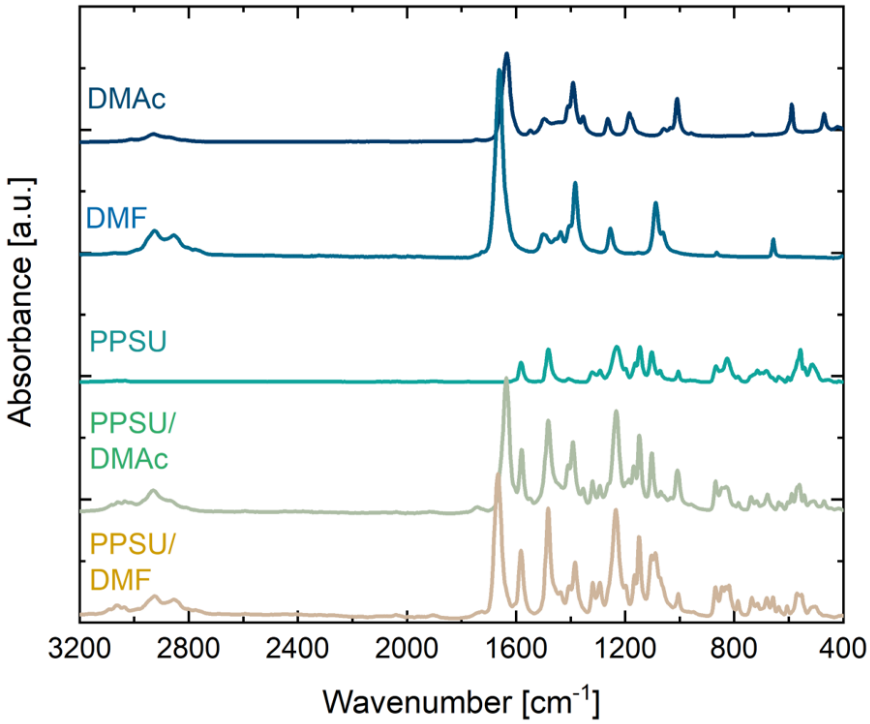

Figure SI 6. Absorbance spectra of PPSU crystals and the native components, measured via FTIR.

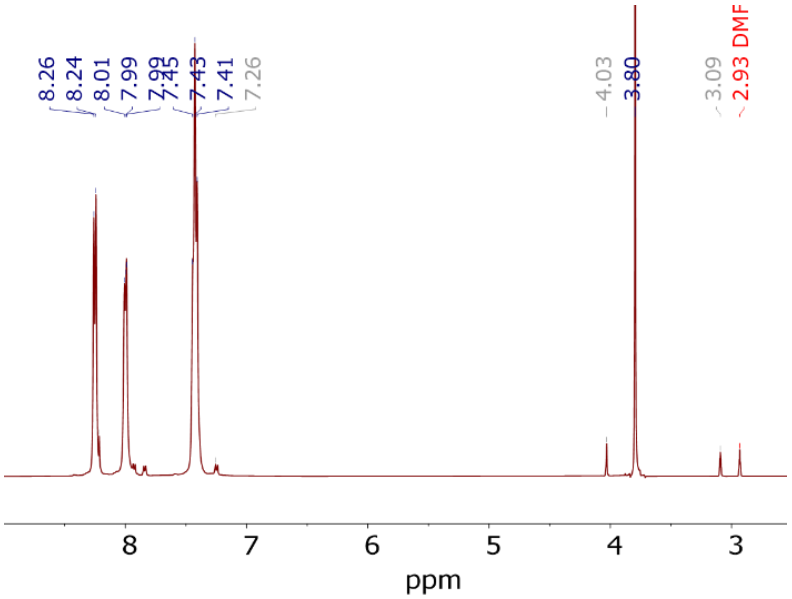

Figure SI 7. ^{1}H NMR spectra with peak identification for PPSU in DMF.

^{1}H NMR (500 MHz, DMF) δ 8.26, 8.24, 8.21, 8.01, 8.01, 7.99, 7.99, 7.44, 7.43, 7.41, 7.26, 4.03, 3.80, 3.09, 2.93.

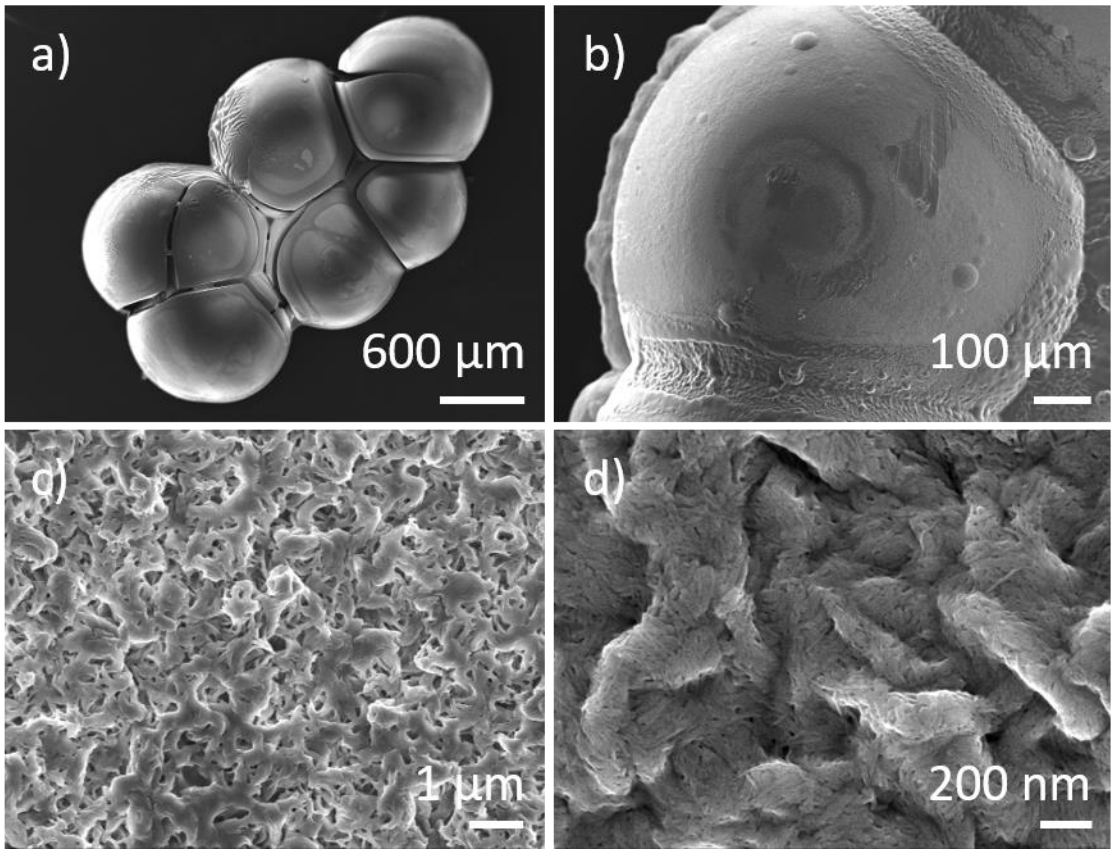

Figure SI 8. SEM micrographs of PPSU spherulites, grown in DMAc.

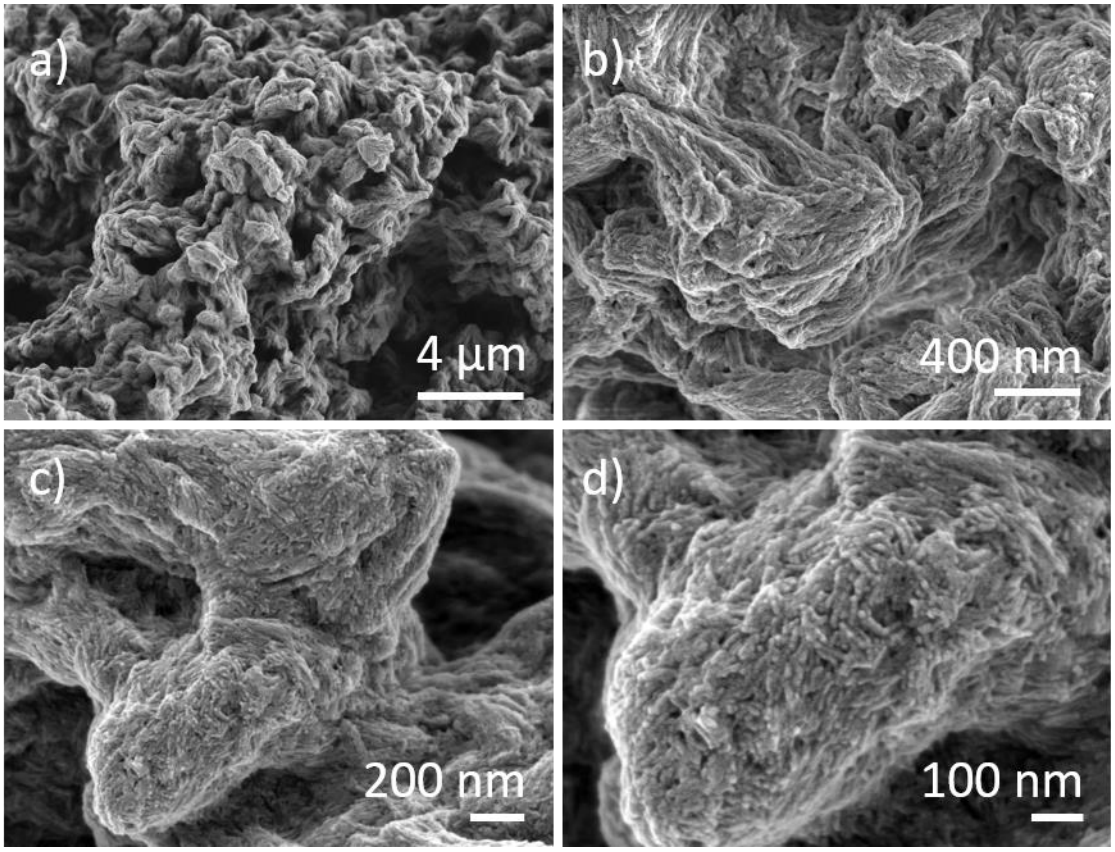

Figure SI 9. SEM micrographs of PPSU crystals, grown in DMF.